

Effect of Clay Modification on the Morphology and the Mechanical/Physical Properties of ABS/PMMA Blends

Tayebe Nazari, Hamid Garmabi, Ahmad Arefazar

Department of Polymer Engineering and Color Technology, Amirkabir University of Technology, Tehran, Iran

Received 3 August 2011; accepted 3 February 2012

DOI 10.1002/app.36953

Published online in Wiley Online Library (wileyonlinelibrary.com).

ABSTRACT: The effect of three types of organoclays on the morphology and mechanical properties of lower critical solution temperature-type poly(acrylonitrile-butadiene-styrene)/poly(methyl methacrylate) (ABS/PMMA) blends was investigated. Polymers were melt-compounded with 2 and 4 wt % of clays using a twin-screw extruder. X-ray scattering and transmission electron microscopy revealed that the intercalation of the nanoclay in the hybrid nanocomposite was more affected by the polarity of the organoclay. Although the morphology of the blends varied by PMMA content, scanning electron microscopy showed smaller PMMA domains for the hybrid systems containing clay par-

ticles. Although good dispersion of the nanoclay through the ABS matrix and at the blend interface led to enhancement of tensile strength, the increment of the stiffness was more noticeable for nanocomposites including less polar organoclay. Well-dispersed clay platelets increased the glass transition temperature. In addition, nanoscratching analysis illustrated an improvement in scratch resistance of ABS because of the presence of PMMA and organoclay. © 2012 Wiley Periodicals, Inc. *J Appl Polym Sci* 000: 000–000, 2012

Key words: ABS/PMMA hybrid nanocomposite; morphology; mechanical properties; T_g ; scratch resistance

INTRODUCTION

In the late 1950s, along with researches about toughening of styrene and styrenic polymers, poly(acrylonitrile-butadiene-styrene) (ABS) was commercialized.¹ A continuous styrene-co-acrylonitrile (SAN) matrix containing SAN-grafted butadiene particles has developed as ABS. Good mechanical performance and processability have made ABS as one of the most applicable engineering thermoplastics. Therefore, the major purpose of ABS compounding (with fillers or other polymers) is usually to improve its thermal properties.

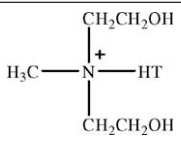
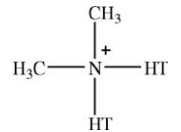
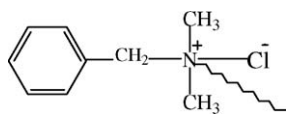
Blends of ABS with poly(methyl methacrylate) (PMMA) and their structural, rheological, and mechanical properties have been investigated extensively.^{2–5} As grafted rubber particles in ABS contain numerous SAN chains on their surfaces, the compatibility and phase behavior of ABS/PMMA blends depend on the affinity of SAN and PMMA components.^{2–4,6} SAN/PMMA blends exhibit a lower critical solution temperature-type phase behavior and have good miscibility as acrylonitrile content of SAN varies in the range of 9–33 wt %.^{7,8} Therefore, coextruded sheets of ABS and PMMA benefit excellent interfacial adhesion because of the miscibility and

molecular interdiffusion of SAN and PMMA at the interface.⁶

PMMA presents good scratch resistance because of being glossy, having good stiffness, and high scratch depth recovery, and as a result, offering low scratch visibility.^{9,10} In contrast, ABS plastics used in the electronic products or interior parts of automobiles tend to be scratched during normal usage or molding process. To avoid this problem, the surface of the ABS objects can be coated or coextruded with scratch-resistant acryl resin like PMMA.¹¹ Although blending of ABS with PMMA can improve the scratch resistance of ABS, it is not superior.¹² The addition of appropriate and well-dispersed hard nanofillers like organoclay to this blend may improve the scratch behavior.¹³ Recently, polymer-blend nanocomposite has attracted great interest.^{14–34} The incorporation of a nanofiller, like organoclay, can increase the compatibility of the blend components by decreasing the total free energy of mixing.^{17,18} In detail, whenever nanoparticles are located in the matrix phase, they improve the dispersion of minor component by preventing the coalescence of the dispersed domains¹⁹ or increasing the matrix viscosity significantly.^{20–23} In contrast, when they have more affinity with the minor phase, usually coarsening the morphology will happen.^{24–27} When nanoclays exist at the interface,^{21,29,30} *in situ* grafting²⁸ and reducing the interfacial tension are other mechanisms for enhancing blend miscibility. However, in addition to thermodynamics, the final morphology is governed by kinetic

Correspondence to: H. Garmabi (garmabi@aut.ac.ir).

TABLE I
Structure and Properties of OMMTs

OMMT name	Organic modifier	CEC (mequiv/100 g)	d_{001} spacing (nm)
C30B		90	1.85
C20A		95	2.45
Nanofil SE3010		40–42 (wt %)	3.6

factors such as blending sequence, shear stress level, and mixing time.^{31–33} The quality of dispersion and the organoclay localization are predominant factors for the property improvement. It seems that the best stiffness and toughness (tensile strength and strain at break) originate from well-dispersed clay throughout both the matrix and the interface.³⁴ However, stress and strain at break are much more affected by the interfacial adhesion.^{23,24,31} In this line, Lee et al.³⁵ studied hybrids of PMMA/SAN with different nanoclays. They observed that the clay platelets were mainly located at the interface of PMMA/SAN. Moreover, cloisite 25A nanoclay appeared to show better dispersion and finer PMMA domains. Shumsky et al.³⁶ examined the effect of nanofillers on the rheological properties and phase separation temperature of PMMA/SAN. Clay cloisite 30B made the blend more miscible and increased the phase separation temperature. Some reports have also developed the ABS blends based nanocomposites such as ABS/PP/clay,²¹ ABS/PA6/clay,²⁶ ABS/PBT/clay,³⁷ and ABS/PC/clay hybrid nanocomposites.³⁸

In this work, the structural and mechanical properties and the scratching behavior of the ABS/PMMA/clay hybrid nanocomposites, prepared using a corotating twin-screw extruder, are presented. To investigate the simultaneous effect of three types of organoclays with different PMMA contents (10, 25, and 40 wt %) and clay loadings (0, 2 and 4 wt %) on the tensile properties, the experiments were designed using response surface methodology (RSM). Furthermore, morphology, dynamic mechanical and thermal behavior, and scratch resistance of ABS/PMMA-based nanocomposites have been studied as well.

EXPERIMENTAL

Materials

ABS (ABS-75), with 25 wt % of acrylonitrile and 18 wt % of butadiene, was purchased from Ghaed Bassir Petrochemical Products, Iran. The PMMA (acryrex CM-205) was prepared by Chi Mei, Taiwan. Commercial organically modified montmorillonites (OMMTs) with different polarities and organic modifiers, Cloisite[®] 30B (C30B) and Cloisite[®] 20A (C20A) from Southern Clay Products and Nanofil[®] SE3010 from Süd-Chemie Company, were also used. The main characteristics of these OMMTs are listed in Table I.

Preparation

ABS/PMMA/nanoclay hybrid nanocomposites were prepared using a laboratory-scale corotating twin-screw extruder manufactured by Coperion, Germany (ZSK25, $L/D = 40$) at a temperature profile of 200–220°C and a screw speed of 300 rpm. Before melt blending, all components were dried at 85°C for 15 h and then fed into the hopper of the extruder at a feeding rate of 5 kg/h. Extruded strands were chopped up into granules and then injection molded into dumbbell-shaped test specimens at melt temperature of 245°C.

To prepare nanocomposites at three different PMMA levels (10, 25, and 40 wt %) and at three clay contents (0, 2, and 4 wt %), the recipes were designed using the RSM. Table II illustrates the composition of the prepared samples in accordance to RSM. RSM is a collection of mathematical and statistical techniques useful for the modeling and the analysis of problems in which several variables influence a target response.^{39,40} Analyzing different responses, RSM depicts responses as a function of assumed variables and represents models to estimate the responses continuously. The trial version of Design Expert 8.0 software was used to carry out the RSM analysis.

TABLE II
Formulation of the Hybrid Nanocomposites According to the Response Surface Method of Experimental Design

No.	Clay type	Clay (%)	PMMA (%)
R1	–	0	10
R2	C20A	2	25
R3	–	0	25
R4	C30B	2	40
R5	C30B	2	10
R6	C20A	2	25
R7	C30B	4	25
R8	C20A	2	25
R9	SE3010	2	10
R10	C20A	4	10
R11	SE3010	4	25
R12	C30B	4	10
R13	C20A	4	40
R14	SE3010	2	40
R15	–	0	40

To evaluate the organoclay interaction with the polymeric components, nanocomposites of ABS/C20A, ABS/C30B, ABS/SE3010, PMMA/C20A, PMMA/C30B, and PMMA/SE3010 with 4 wt % of clay were prepared in an internal mixer (Brabender DSE25, Germany). The mixing time, temperature, and rotor speed of blending process were set at 12 min, 210°C, and 90 rpm, respectively.

Characterization

Tensile test was carried out using a Galdabini Su 2500, Italy apparatus at a crosshead speed of 50 mm/min. Dynamic mechanical analysis (DMA) was carried out using the Thermal Analyst 2000 (Du Pont, USA) to measure the dynamic modulus and damping factor as a function of temperature. The sample bars (sizes = $4 \times 1.5 \times 0.45 \text{ cm}^3$) were heated at 2°C/min from 25 to 140°C in a single cantilever bending mode at a frequency of $\omega = 1 \text{ Hz}$. Using a Hysitron Inc. TriboScope1 Nanomechanical Test Instrument, USA with a Berkovich three-sided pyramidal diamond indenter ($R = 200 \text{ nm}$), nanoscratch tests were performed on the slice of the injection-molded specimens (size = $1 \times 1 \text{ cm}^2$). The scratched specimens were firmly mounted on an AFM stage of a Nanoscope III instrument, USA for direct measurement of the initial surface and the final impression, using the same indenter tip. Constant force (400 μN) nanoscratchings of 4 μm length were performed within 30 s at constant rate after the initial indentation. At least three replicates were carried out for each sample. Rheological measurements were performed by a UDS 200 Paar Physica rheometer, USA with parallel-plate geometry (with 25 mm diameter and 1 mm gap). Isothermal dynamic frequency sweep experiments were carried out at strain of 1% and temperature of 245°C to study the linear viscoelastic properties. Wide-angle X-ray diffraction (XRD) patterns were recorded on a Phillips X'Pert diffractometer using Co $K\alpha$ radiation ($\lambda = 0.178 \text{ nm}$). The diffractometer, Netherlands operated at a voltage of 40 kV and a current of 30 mA. Data were obtained from $2\theta = 1^\circ\text{--}10^\circ$ at a scanning speed of $0.04^\circ/\text{s}$ at room temperature.

The surfaces of molded specimens were observed using a Hitachi S-416, Japan (FE-SEM) scanning electron microscope after sputter gold coating. The samples were cryogenically fractured and etched with a permanganic etching agent (solution containing 0.7 g of KMnO_4 , 20 mL of concentrated sulfuric acid, and 20 mL of phosphoric acid) to visualize PMMA and polybutadiene in ABS matrix.⁴¹ The surface of the specimens was immersed into the prepared solution for 15 min and then washed in running water. Transmission electron microscopy (TEM) observations of ultrathin sections (60–70 nm) were performed using a Philips EM 208S TEM with 100 kV accelerating

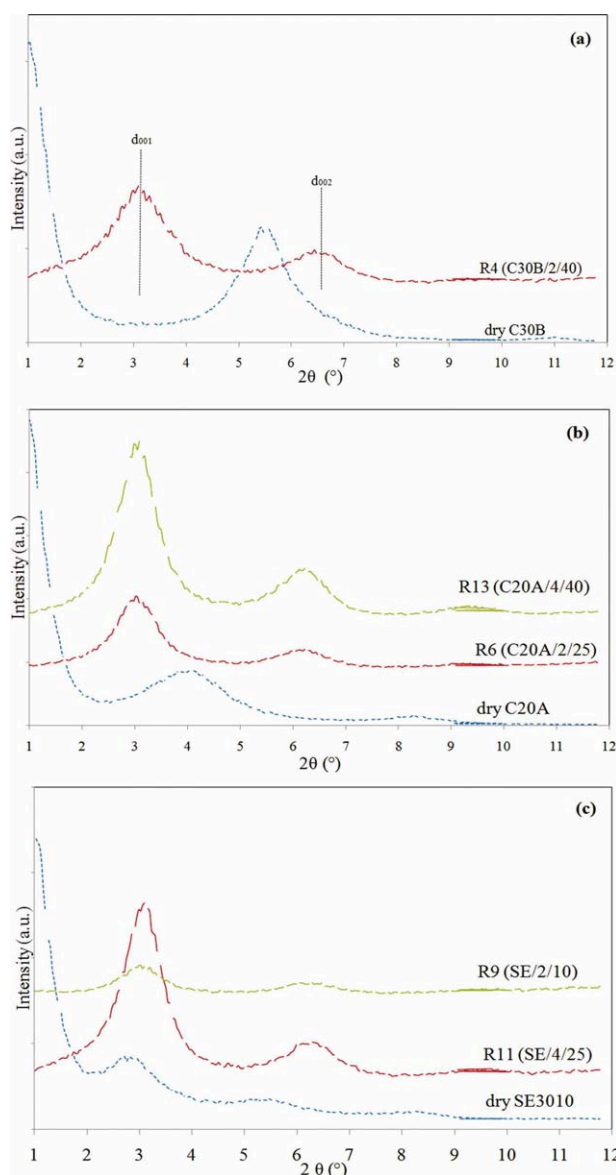


Figure 1 X-ray diffraction patterns of ABS/PMMA/clay nanocomposites for three different clays: (a) C30B, (b) C20A, and (c) Nanofil SE3010. [Color figure can be viewed in the online issue, which is available at wileyonlinelibrary.com.]

voltage. Ultrathin slices were prepared with a Reichert OMU3 ultramicrotome in liquid nitrogen.

RESULTS AND DISCUSSION

Clay dispersion

XRD is commonly used to characterize the interlayer spacing of clay particles, which is correlated with their intercalation level. As the polymer chains are intercalated, the gallery spacing increases, resulting in a shift of characteristic reflections to lower angles. XRD patterns of some ABS/PMMA/clay nanocomposites are shown in Figure 1(a–c). As observed, the peak position of $2\theta = 5.6^\circ$ ($d_{001} = 1.82 \text{ nm}$) for Clay

TABLE III
XRD Results for Polymer/Clay Nanocomposites

Sample	2 θ value ($^{\circ}$)	d -spacing (nm)	Δd (nm)
C30B	5.6	1.82	–
ABS/C30B	3.27	3.135	1.31
PMMA/C30B	3.18	3.22	1.4
C20A	4	2.55	–
ABS/C20A	3.23	3.17	0.62
PMMA/C20A	3.35	3.06	0.51
SE3010	2.83	3.62	–
ABS/SE010	3.17	3.23	–0.39
PMMA/SE010	3.27	3.16	–0.46

C30B decreased to 3.23 $^{\circ}$ (3.16 nm) in sample R4, containing 40 wt % of PMMA and 2 wt % of C30B [Fig. 1(a)]. In this sample (and other hybrids of C30B, not shown here), the presence of the second peak of d_{002} may point to ordered intercalated nanocomposite structure as stated by Vaia and Giannelis.⁴² Moreover, in the hybrids of clay C20A, the main diffraction peak at 4 $^{\circ}$ (2.55 nm) shifts to lower angles of 3.1 $^{\circ}$ (3.29 nm) and 3 $^{\circ}$ (3.4 nm) [Fig. 1(b)]. Conversely, in the hybrids of clay SE3010, very small differences between diffraction peaks of nanoclay at 2.83 $^{\circ}$ (3.62 nm) and nanocomposites at 3.2 $^{\circ}$ (3.2 nm) and 3.1 $^{\circ}$ (3.29 nm) are observed [Fig. 1(c)]. However, these represent no intercalation. Clay SE3010 is more organically modified than both of C20A and C30B clays.⁴³ This OMMT contains the aromatic ring in the organic modifier that is compatible with aromatic rings of the styrene of the ABS phase. In addition, commercial clay Cloisite 10A is organically modified with the similar aromatic organic modifier and represented intercalation in ABS/Cloisite 10A^{44,45} and PMMA/Cloisite 10A⁴⁶ nanocomposites. However, this discrepancy may be attributed to melt-blending process at high temperatures (more than 200 $^{\circ}$ C) and removal of intercalant agent molecules from clay galleries. As shown, clay C30B depicts more intercalation ($\Delta d = 1.34$) than other OMMTs, which is consistent with rheological observation (not shown here) and other reports about ABS/clay,^{44,47} PMMA/clay,⁴⁶ and SAN/PMMA/clay⁴⁸ nanocomposites.

The XRD results of individual polymer nanocomposites, ABS/clay, and PMMA/clay are summarized in Table III. In spite of different polarities and initial gallery spacings of OMMTs, a roughly similar increase of the interlayer spacing of C30B and C20A may be noticed for both of the neat matrices. Moreover, both ABS and PMMA illustrate no intercalation with SE3010. These results indicate that both polymers have the same affinity for intercalation with OMMTs, and consequently, predominant localization of the filler might be at the interface, which has been reported in PP/PS/C20A,²¹ PMMA/PC/C20A,²² and PA6/PVDF/C20A³⁴ nanocomposites. However,

Filippone et al.⁴⁹ observed exactly the same increase in d -spacing for LDPE/clay and PA11/clay nanocomposites; nevertheless, differential scanning calorimeter analysis illustrated minor enhancement of melting temperature of PA11 phase in LDPE/PA11/clay system. In agreement, TEM observations showed localization of clay in PA11 phase. Thus, besides XRD technique, a complementary method is necessary for analyzing nanoclay location in a polymer blend.

Although DMA examination has demonstrated one glass transition temperature (T_g) for ABS/PMMA/clay hybrids (discussed later), rheological analyses were performed to exemplify interaction of

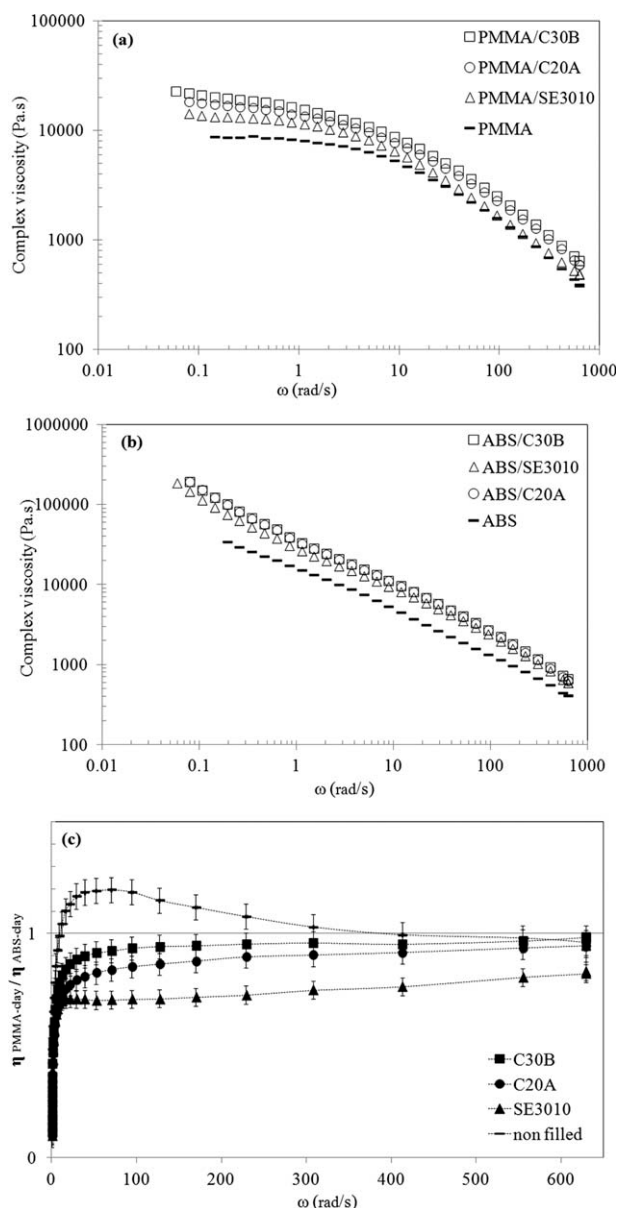


Figure 2 Plots of complex viscosity versus angular frequency for (a) PMMA/clay, (b) ABS/clay nanocomposites, and (c) viscosity ratio of PMMA–clay/ABS–clay.

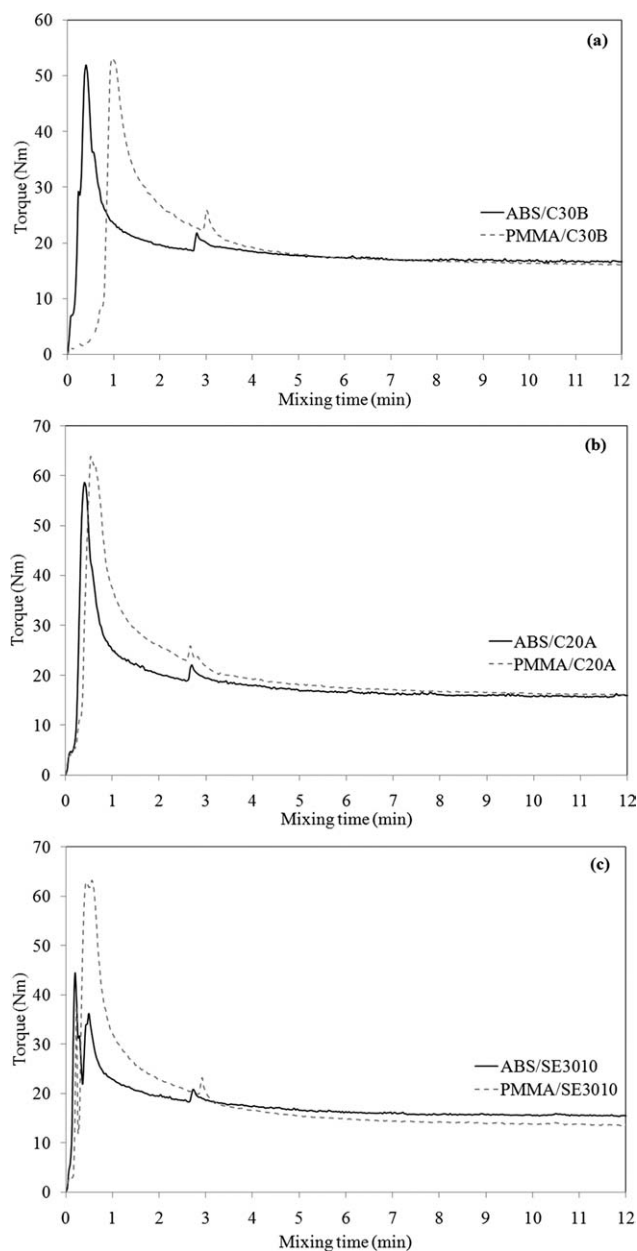


Figure 3 Torque development of (a) ABS/C30B, PMMA/C30B, (b) ABS/C20A, PMMA/C20A, and (c) ABS/SE3010, PMMA/SE3010 nanocomposites through the mixing process in the internal mixer at 210°C.

the neat polymers with OMMTs [Fig. 2(a–c)]. Clay C30B presents more viscosity enhancement in PMMA than other OMMTs [Fig. 2(a)]; however, the viscosity curve intersects with PMMA/C20A viscosity curve at frequency values higher than 100 rad/s. It seems that both C30B and C20A clays show evidence of similar interaction with PMMA as well as with ABS in all frequency ranges, 0.01–600 rad/s [Fig. 2(b)]. Figure 2(c), which shows the viscosity ratio of PMMA–clay to ABS–clay, indicates better evaluation of viscosity improvement. As can be seen, polymers and nanocomposites containing C20A and

C30B exhibit approximately the same viscosity ratio close to unity at higher frequencies, which can represent the mixing conditions. Moreover, the torque–time variation curves during the mixing of ABS/clay and PMMA/clay nanocomposites in the internal mixer [Fig. 3(a–c)], which were calculated from the electrical current, are closely related to the viscosity of each system. As the viscosity ratio of used polymers, ABS and PMMA, was near one, the torque differences are not very significant. However, torque values of composites after clay addition ($t = 3$ min) are exactly the same, as shown in Figure 3(a–b). As a result, interfaces are the most probable location of

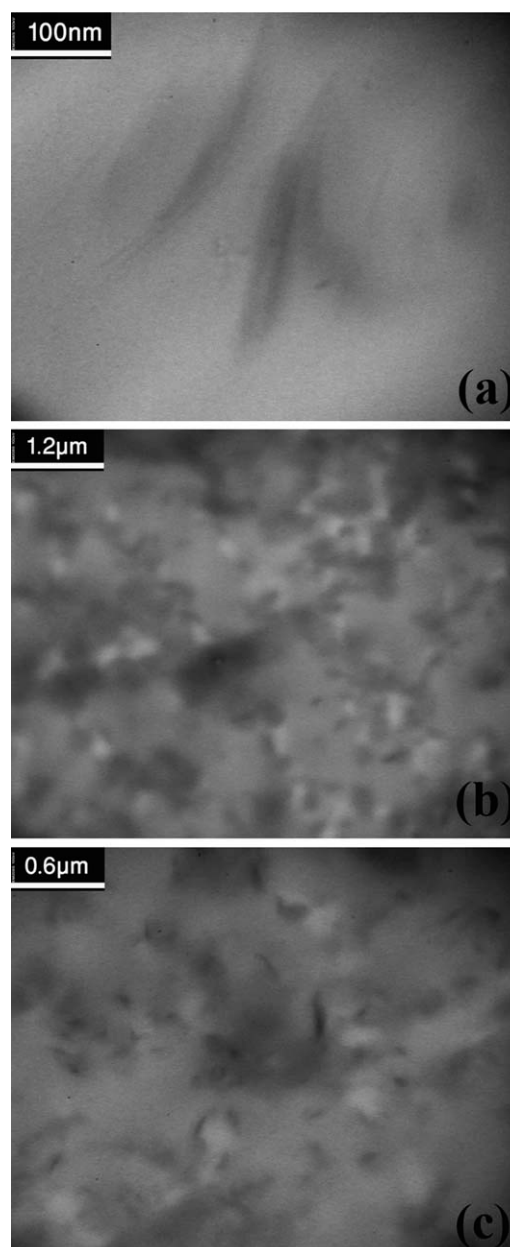


Figure 4 TEM images for hybrid sample R6 containing 2 wt % of C20A: (a) 100 nm, (b) 1.2 μm, and (c) 0.6 μm scales.

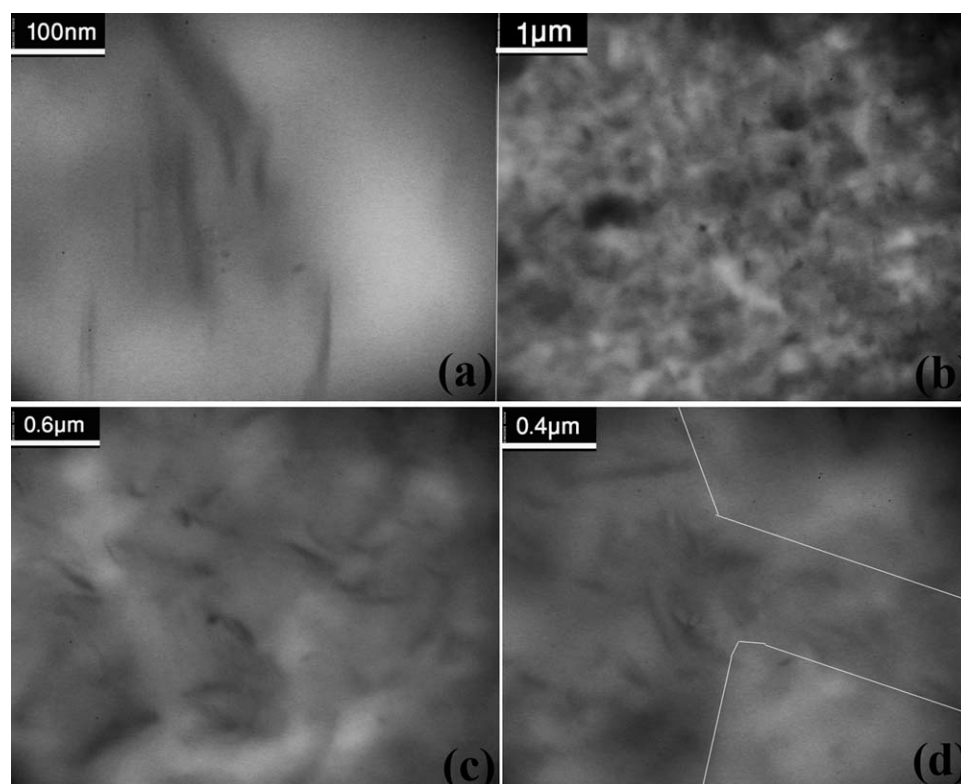


Figure 5 TEM images for hybrid sample R7 containing 4 wt % of C30B: (a) 100 nm, (b) 1 μm , (c) 0.6 μm , and (d) 0.4 μm scales.

C20A and C30B in ABS/PMMA/clay hybrids. Although nonintercalated ABS/SE3010 nanocomposite displays higher torque and viscosity enhancement than PMMA/SE3010 ($\eta_{\text{PMMA-SE3010}}/\eta_{\text{ABS-SE3010}} < 1$), dispersion of clay SE3010 in ABS phase is predominant.

Figure 4(a–c) shows the TEM images of sample R6 containing 25 wt % of PMMA and 2 wt % of C20A in ABS/PMMA/clay hybrid. Brighter continuous domains represent PMMA phase. Magnified image [Fig. 4(a)] demonstrates the intercalated structure of OMMT, and further images [Fig. 4(b,c)] show the existence of clay particles in SAN phase (darker domains) at the boundary of butadiene particles (light spheres) and close to the interfaces of ABS/PMMA. Figure 5(a) illustrates the intercalated structure of C30B in sample R7 (ABS/PMMA/OMMT, 75/25/4 wt %). In addition, the presence of thin clay platelets in this picture indicates intercalated/exfoliated structure of hybrid nanocomposites. It seems that with the increasing clay loading, clay particles are localized within all phases (matrix, dispersed phase, and interface) [Fig. 5(b)]. On the other hand, Figure 5(c,d) shows the presence of nanoparticles in ABS matrix and next to the interfaces. Lee et al.³⁵ observed that for PMMA/SAN nanocomposites including 5 wt % of nanofillers, unmodified clay Cloisite Na⁺ are more existed at the interfaces and also in PMMA droplets. Besides, the organomodified

MMT particles, Cloisite C25A (CEC = 95 mequiv / 100 g clay), were located in SAN matrix as well as at the interface. Polarity and interlayer spacing of clay C30B (CEC = 90 mequiv/100 g clay) lay between ones of Cloisite Na⁺ and Cloisite C25A; therefore, the presence of PMMA domains including nanoclay particles in hybrid nanocomposites containing 4 wt % of C30B is not unexpected. It is also noticeable that the clay location may change with the clay content. For instance, it is reported in PE/PBT/clay²⁹ and PCL/PEO/clay³⁰ nanocomposites that at low clay content (<2 wt %), clay particles were placed at the interface as they are thermodynamically stable with minimum chemical potential; however, they migrated to some extent into desirable phase at higher clay contents (5 wt %). This phenomenon recalls the critical micelle concentration of a compatibilizer in a polymer blend. Therefore, it can be deduced that 2 wt % of clay C30B and also C20A layers (resulted from XRD and viscosity measurements) will be placed at the interface; however, they may migrate into the dispersed phase at a concentration higher than the critical one.

Morphology

The impact of the nanoclay distribution on the microstructure of the blends was examined by SEM analysis combined with extraction experiments using

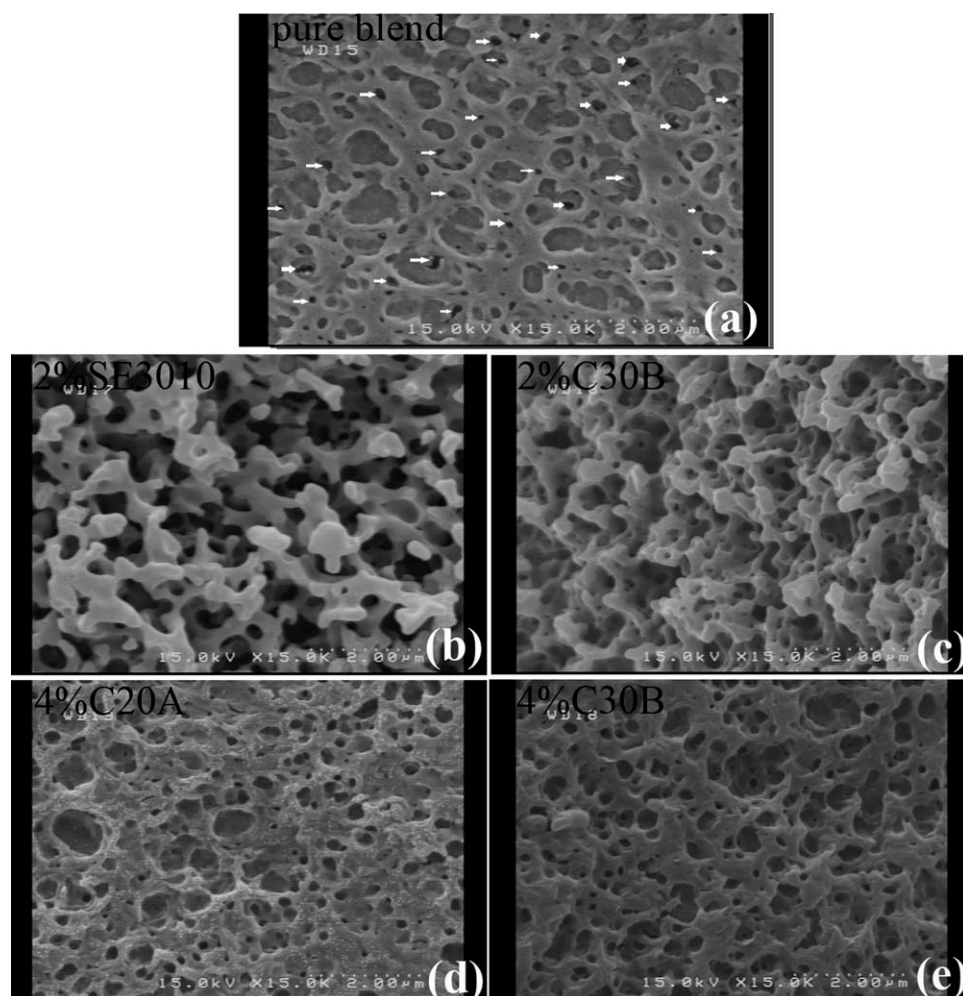


Figure 6 SEM micrographs of hybrid samples containing 10 wt % of PMMA: (a) R1, (b) R9, (c) R5, (d) R10, and (e) R12 (2 μm scale). The butadiene and PMMA phase were removed by permanganic etching solution.

permanganic etching agent. The comparison of the SEM pictures of the unfilled and OMMT-filled 90/10 ABS/PMMA blends is shown in Figure 6. The unfilled blend exhibits matrix-dispersed morphology with large PMMA droplets [Fig. 6(a)]. In addition, extracted butadiene particles were observed in both PMMA and ABS phases, some of which are marked with white vectors. Because butadiene particles are being surrounded by grafted SAN chains, their migration into PMMA will take place.²⁻⁴ Although the addition of 2 wt % of C30B and SE3010 causes a considerable reduction of the PMMA particle size, clay C30B produces smaller particles than SE3010 [Fig. 6(b,c)]. This observation is attributed to better interactions of clay C30B localizing at the interface, and as a result, compatibilizing effect of the nanoclays. In the case of clay SE3010, better interaction with ABS and viscosity improvement of matrix leads to decrease in the droplet size. As clays C30B and C20A show similar affinity to both polymers, 90/10 ABS/PMMA blend depicts nearly the same dispersed domains size in the presence of 4 wt % of

them [Fig. 6(d,e)]. Moreover, uneven distribution of droplets size because of the migration of clay platelets to some extent from interface into droplets is observed in Figure 6(d,e), which is in agreement with the TEM results. Localization of the clay particles in the PMMA domains increases the viscosity and may cause coalescence and enlargement of droplets.

Because of the high processing temperature and the injection molding of samples (higher than phase separation temperature $\sim 200^\circ\text{C}$), the blend of 75/25 ABS/PMMA demonstrates co-continuous phase structure [Fig. 7(a)]. SEM image of sample R7 including 4 wt % of clay C30B shows mixed morphology [Fig. 7(b)], which verifies the results obtained from TEM micrographs. Dispersion of C30B prevents the coalescence of droplets and results in dispersed matrix morphology in some areas. On the other hand, existence of co-continuous structure with enlarged PMMA phases is clear in the other areas. The addition of 2 wt % of C20A, mainly located at the interface, and 4 wt % of SE3010, located in the matrix,

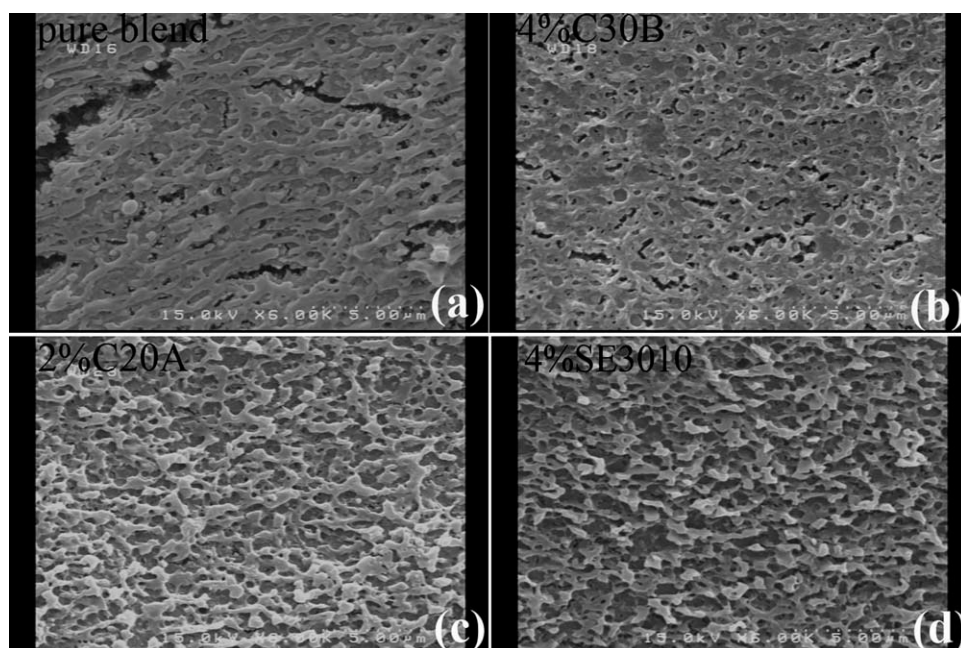


Figure 7 SEM micrographs of hybrid samples containing 25 wt % of PMMA: (a) R3, (b) R7, (c) R6, and (d) R11 (5 μm scale). The butadiene and PMMA phase were removed.

promotes a drastic size reduction in co-continuous phases, resembling primary stages of phase separation process [Fig. 7(c,d)]. Therefore, compatibilization and phase separation retardation in the presence of OMMTs in 75/25 ABS/PMMA hybrid can be deduced.

Figure 8(a–c) illustrates the morphology of 60/40 ABS/PMMA blend and nanocomposites. As observed, all 60/40 hybrids display co-continuous microstructure. Moreover, the addition of 2 wt % of clays C30B and SE3010 minimize co-continuous domains size owing to compatibilizing effect of the nanoclays.

Tensile properties

An empirical model applying multiple regression analysis is supposed to estimate theoretical responses in RSM. The second-order model has been used to describe the tensile properties (modulus and tensile strength) as responses of variables in this study, which is given by the following equation:

$$\eta = \beta_0 + \beta_1x_1 + \beta_2x_2 + \beta_3x_3 + \beta_{11}x_1^2 + \beta_{22}x_2^2 + \beta_{33}x_3^2 + \beta_{12}x_1x_2 + \beta_{13}x_1x_3 + \beta_{23}x_2x_3 \quad (1)$$

where β_{ii} is the curvature term of independent variables and β_{ij} is the interaction coefficient between variables x_i and x_j . Fifteen experiments, including three levels for each parameter, allow fitting a quadratic response surface model as a function of clay type, clay loading, and PMMA content.

The results obtained from the tensile test are summarized in Table IV. By linear regression analysis of

eq. (1) for modulus of the prepared compounds, the coefficient values of the fitted model are shown in Table V. The R^2 value of 88% demonstrates that the model is able to predict 88% of the modulus variations in the variable domains. Furthermore, a quadratic model with 98.7% R^2 value and a linear model with $R^2 = 93.9\%$ can be fitted for the results of tensile strength. The linear model of tensile strength is given by the following equation:

$$\sigma_y = 42.69 + 0.22x_1 + 0.38x_2 - 1.56x_3 \quad (2)$$

where x_1 , x_2 , and x_3 represent PMMA content, clay loading, and clay type, respectively. According to the RSM, the coded numbers of -1 , 0 , and 1 were used for parameter x_3 that represent clays C30B, C20A, and SE3010, respectively.

Using the second-order models obtained from RSM, modulus and tensile strength levels for 12 nonprepared samples were predicted. Figure 9(a–c) shows the mechanical properties as a function of PMMA content for all samples. It is noteworthy to mention that in a full-factorial designed experiment, to evaluate the effect of three factors varying in three levels on the property, we ought to prepare $3^3 = 27$ samples through melt compounding. However, using RSM made it possible to prepare 15 samples and to predict the responses for other 12 ones.

Modulus

In the ABS/PMMA hybrid blends, modulus increases by increasing the PMMA content, which

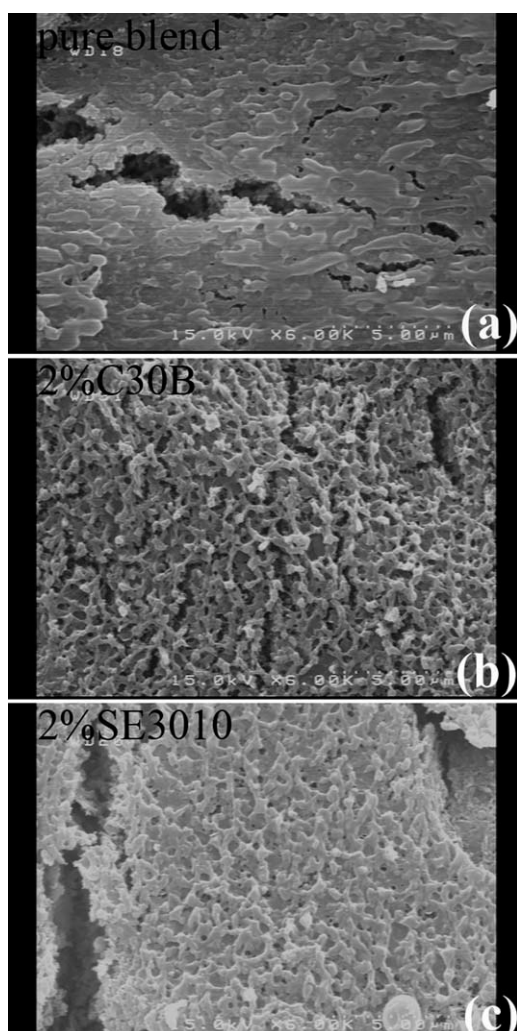


Figure 8 SEM micrographs of hybrid samples containing 40 wt % of PMMA: (a) R15, (b) R4, and (c) R14 (5 μm scale). The butadiene and PMMA phase were removed.

shows various behaviors by adding the OMMTs in different levels of PMMA [Fig. 9(a)]. The incorporation of 2 wt % of clay SE3010 into 90/10 ABS/PMMA reduces the modulus because of nonintercalated structure and poor dispersion. This content of clays C30B and C20A enhances the modulus because of good dispersion; however, the enhancement is not significant while nanoparticles are located at the interface.^{21,24} Increasing the clay content improves the stiffness, whereas the sample containing 4 wt % of SE3010 shows unexpected high stiffness. At 25 wt % of PMMA content, all clays improve the modulus regardless of the clay loading and dispersion quality. However, the effect of 4 wt % of SE3010 is outstanding. All 60/40 ABS/PMMA-filled blends present lower stiffness when compared with the pure blend, yet 4 wt % of SE3010 filled one is an exception. As the PMMA viscosity is lower than ABS viscosity at high shear rates of mixing process [Fig. 3(c)], increasing the PMMA content may increase the

TABLE IV
Tensile Properties of Prepared Compounds

Sample	Modulus (MPa)	Elongation at break (%)	Tensile strength (MPa)
R1	2723 \pm 192	10 \pm 4	45 \pm 0.2
R2	3055 \pm 20	20 \pm 8	50 \pm 0.1
R3	2915 \pm 49	14 \pm 6	48 \pm 0.6
R4	2831 \pm 51	21 \pm 5	53 \pm 0.7
R5	2813 \pm 26	26 \pm 11	47 \pm 0.3
R6	3273 \pm 414	14 \pm 2	49 \pm 0.7
R7	3073 \pm 103	16 \pm 7	50 \pm 0.7
R8	2989 \pm 61	21 \pm 6	50 \pm 1
R9	2620 \pm 75	19 \pm 7	43 \pm 0.6
R10	2837 \pm 3	12 \pm 1	47 \pm 0.2
R11	3535 \pm 37	13 \pm 2	47 \pm 0.5
R12	2896 \pm 38	7 \pm 2	48 \pm 0.6
R13	3108 \pm 287	9 \pm 1	54 \pm 0.3
R14	2935 \pm 208	24 \pm 9	51 \pm 0.1
R15	3189 \pm 60	16 \pm 3	53 \pm 0.1
ABS	2265 \pm 18	14 \pm 4	45 \pm 0.7
PMMA	2563 \pm 178	1.3 \pm 0.3	–

migration of clays C30B and C20A into PMMA phase; however, these two clays present similar interaction with both polymers. As a reason, stiffness reduces by localization of clays within the dispersed phase owing to shear-induced migration.³² As mentioned, this type of movement is not possible for clay SE3010 while owning nonintercalated stacks. Therefore, SE3010 nanoparticles disperse in the matrix phase and enhance the stiffness. In polymer blend nanocomposites, tensile strength and strain at break are much more affected by the interfacial adhesion; however, it is not a surprise that the modulus is increased by the addition of high-rigidity fillers like nonintercalated SE3010.³¹

Tensile strength

Tensile strength (σ_y) enhances by increment of PMMA content [Fig. 9(b)]. In 90/10 ABS/PMMA

TABLE V
Parameter Estimates and the Statistical Results of Full Quadratic Response Surface Approximation for Modulus of ABS-Based Hybrid Nanocomposites

Term	Estimate	P-value
Constant: β_0	2136.106	0.069
PMMA content: β_1	65.557	0.148
Clay content: β_2	–27.372	0.086
Clay type: β_3	–458.718	0.427
PMMA content \times PMMA content: β_{11}	–1.196	0.017
Clay content \times Clay content: β_{22}	22.007	0.291
Clay type \times Clay type: β_{33}	37.459	0.667
PMMA content \times Clay content: β_{12}	0.044	0.985
PMMA content \times Clay type: β_{13}	5.324	0.256
Clay content \times Clay type: β_{23}	136.409	0.033

P-values less than 0.05 indicate that model terms are significant.

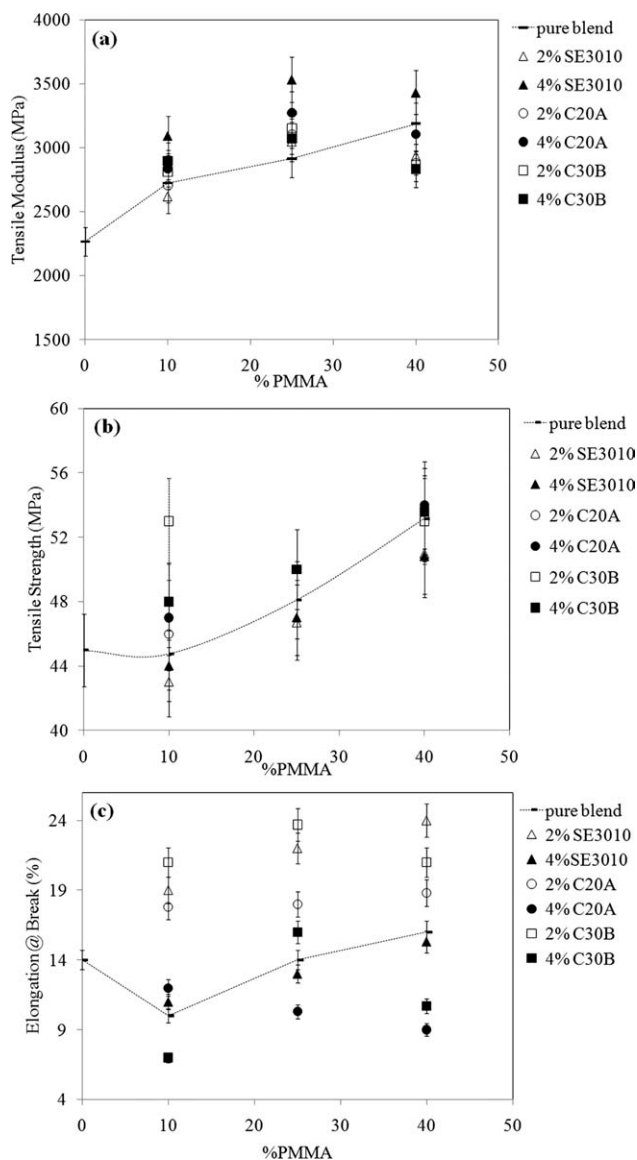


Figure 9 (a) Modulus, (b) tensile strength, and (c) elongation at break of all samples as a function of PMMA content.

hybrids, inclusion of 2 wt % of C30B presents the highest tensile strength. More intercalated structure and superior dispersion of 2 wt % of C30B at the interface, which facilitates the stress transfer between the matrix and the dispersed phase, led to highest interfacial adhesion. Consequently, tensile strength will be enhanced, which is more noticeable at lower amount of PMMA. The incorporation of clay C20A increases the interfacial adhesion and tensile strength as well. However, the addition of clay SE3010, for all clay contents and in all hybrids (75/25 and 60/40 ABS/PMMA), leads to a reduction in tensile strength. It may be concluded that clays C20A and C30B can act as reinforcement nanofillers.

It seems that clay migration into PMMA domains by increasing the clay and PMMA loading in the case of C20A and C30B, deduced from morphologi-

cal results, plays crucial role in modulus and tensile strength of hybrid samples. As nanolayers diffuse into domains, it causes lower enhancement of tensile strength and also reduction of tensile modulus.

Elongation at break

In general, blending of ABS with PMMA increases the formation of crazes during the tensile test,⁵ and therefore, more stress whitening during the test and augmentation of elongation at break was observed [Fig. 9(c)]. Despite the used OMMTs could act as reinforcement or not, it is observed that incorporation of 2 wt % of clay enhances the elongation at break at all PMMA content. However, increasing the clay loading leads to earlier breakage. Various observations have been reported about the effect of clay on the elongation at break in hybrid systems. As OMMT is located at the interface in PP/PS/C20A hybrid system, elongation at break was stated to be improved; however, the lower C20A content presented more increment. In PP-*g*-MA/PS/C20A hybrid blend, while exfoliated clay platelets were dispersed in the matrix, elongation at break was lessened.²¹ In some cases, lack of interfacial adhesion diminished both the tensile strength and the elongation at break.^{23,50} On the contrary, while the clay

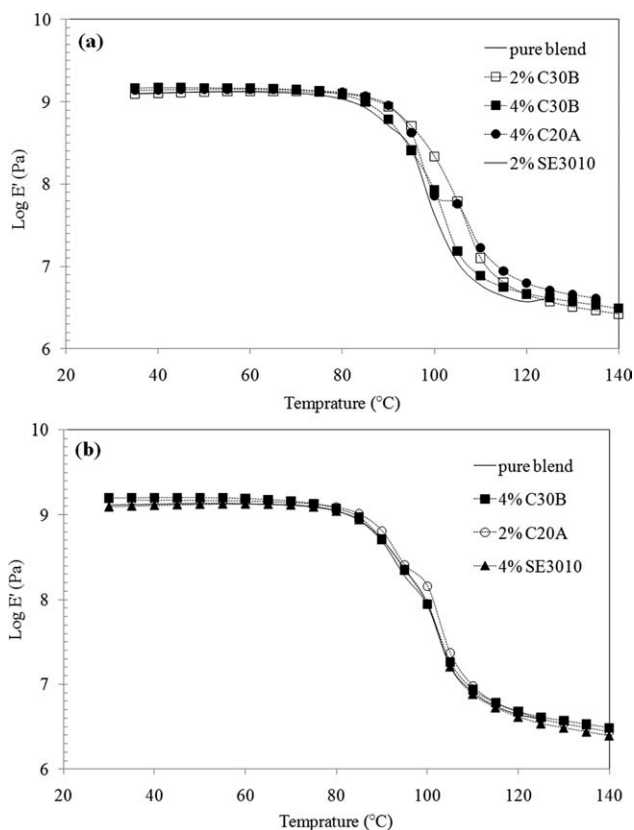


Figure 10 Temperature-dependent storage modulus (Log E') of (a) 90/10 and (b) 75/25 ABS/PMMA hybrid blends.

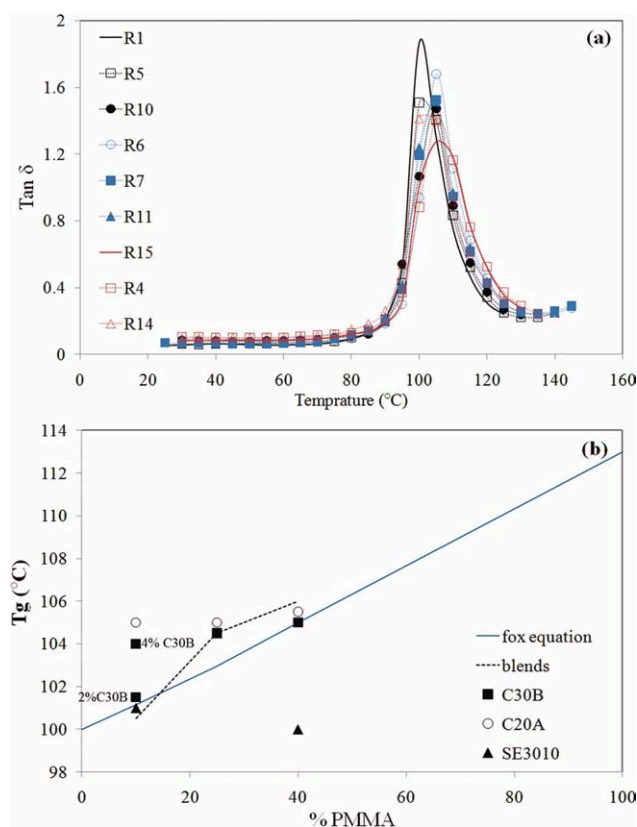


Figure 11 (a) Temperature dependence of $\tan \delta$ and (b) T_g as a function of PMMA content for prepared samples. [Color figure can be viewed in the online issue, which is available at wileyonlinelibrary.com.]

improved the adhesion, the microscopic heterogeneity⁴⁹ or restricted polymer chains mobility caused by the intercalated/exfoliated clay platelets⁵¹ caused elongation failing. In addition, it is believed that at lower contents of nanoclays, nanoparticle orientation and alignment during tensile deformation enhance the toughness. Nevertheless, stress-concentrating effect of agglomerated particles at higher contents reduces the elongation at break of the nanocomposite.⁵² Clays C30B and C20A develop the interfacial adhesion in ABS/PMMA blends. Thus, the later claims (orientation of nanoplatelets at lower content and stress concentration at higher content) are more reliable for ultimate strain behavior.

Dynamic mechanical thermal properties

The thermodynamical mechanical responses of ABS/PMMA blends as a function of OMMTs are examined by DMA measurements. As shown in Figure 10(a,b), the addition of organoclay slightly increases the storage modulus irrespective of clay type and amount. Figure 11(a,b) illustrates the damping factor and glass transition temperatures (T_g). Although the greatest damping factor takes place in the tempera-

ture range of 90–120 °C, it is observed that both one-phase and two-phase samples with co-continuous morphology (containing 25 and 40 wt % of PMMA) represent one T_g . Kumaraswamy et al.⁵³ and Lee et al.³⁵ have reported this observation in SAN/PMMA blends and nanocomposites. Glass transition temperature of ABS and PMMA is 100 and 113 °C, respectively. It has been pointed out that if the difference in T_g s of pure polymers is small (<20 °C), overlapping of the transitions may appear as a single transition.⁵³ Hence, ABS/PMMA blends will show one T_g . Using a mixture law like simple Fox equation, one can predict the T_g s of pure blends. Positive deviation of the experimental T_g from the calculated T_g demonstrates strong interaction of blend components. In Figure 11(b), T_g of 90/10 blend is lower than calculated T_g ; however, blends containing higher amount of PMMA indicate positive deviation from mixture law. The incorporation of clay enhances the interaction and the compatibility of 90/10 ABS/PMMA blend components, and consequently, it increases the T_g s. However, the T_g of strong interacted blends are not affected by clay addition because of their co-continuous morphology. It seems that nonintercalated clay SE3010 exhibited a negative deviation, and therefore, observed T_g was

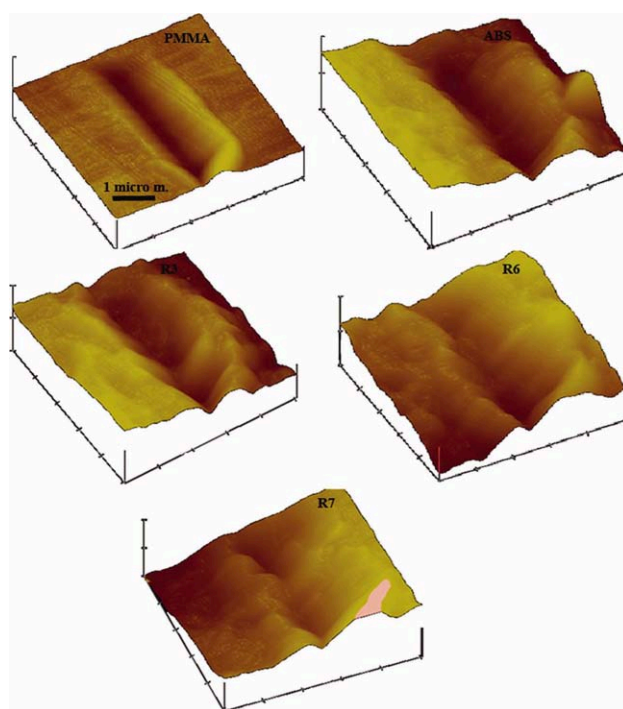


Figure 12 Three-dimensional AFM topographical micrographs showing differences in nanoscratch deformation behaviors of PMMA, ABS, R3 (ABS/PMMA 75/25), R6 (ABS/PMMA/C20A, 75/25/2), and R7 (ABS/PMMA/C30B, 75/25/4) at a $5 \times 5 \mu\text{m}^2$ field of view. [Color figure can be viewed in the online issue, which is available at wileyonlinelibrary.com.]

TABLE VI
Results of Scratch Test for ABS, PMMA, Their Blends, and Hybrids

Sample	Scratched depth (nm)	Residual scratch depth (nm)	Scratch depth recovery (%)	Scratch width (μm)
ABS	325 \pm 20	174 \pm 11	46.5	1.7 \pm 0.03
R3 (ABS/PMMA 75/25)	330 \pm 24	109.4 \pm 24	66.8	1.04 \pm 0.15
R6 (2 C20A/25 PMMA)	300 \pm 20	103.75 \pm 42	65.4	1.29 \pm 0.27
R7 (4 C30B/25 PMMA)	275 \pm 21	88.34 \pm 16	67.9	1.05 \pm 0.17
PMMA	220 \pm 39	61.83 \pm 3	71.9	0.89 \pm 0.11

much smaller when compared with T_g of other samples ($\sim 5^\circ\text{C}$ for 60/40 ABS/PMMA blend).

In spite of better dispersion and interaction of clay C30B with polymeric components, it seems that clay C20A causes higher improvement of T_g in hybrid samples. Higher degree of intercalation and existence of one-layer or two-layer stack of clay C30B might let the modifiers be released into the polymers.³⁵ This may bring about the softening effect and insignificant enhancement of T_g in the presence of clay C30B.

Scratch behavior

Three-dimensional AFM micrographs showing differences in the scratch behavior of the ABS, PMMA, unfilled (R3), and filled blends (R6 and R7) of 75/25 ABS/PMMA at identical scratch conditions are given in Figure 12. Hybrid nanocomposites R6 and R7 contain 2 wt % of clay C20A and 4 wt % of clay C30B, respectively. Because of the viscoelastic behavior of polymeric materials, scratched depth recovers to some extent while scratching tip is sliding on the surface so far. Therefore, AFM images will show the residual scratch depth. It is observed that PMMA displays the smooth scratch subsurface and scratch track with a little piling up on both sides of the scratch width. These indicate the indestructible ductile behavior of PMMA. However, ABS and three hybrid samples illustrate wave-like scratching patterns and noticeable piling up. These waves or asperities on the scratch wall have been attributed to "stick-slip" behavior of almost all polymers (with the exception of PMMA) especially elastomers in sliding type of tests.^{9,54} Stick-slip is contributed to fluctuation of tangential scratch force (sequential accumulation and release) along the scratch length due to the viscoelastic nature of the polymers. By analyzing the scratch images, the scratch width and residual depth of samples were obtained and summarized in Table VI. As can be seen, scratch depth and width in PMMA are the least. In addition, scratch depth recovery is as high as 71.9% more than other samples, which demonstrates self-healing behavior of PMMA.⁹ The blending of ABS with scratch-resistant PMMA improves the scratch resist-

ance of ABS; sample R3 presents the lower scratch width, residual depth, and scratch recovery of around 67% than pure ABS. The incorporation of 2 and 4 wt % of clays C20A and C30B, respectively, which exhibit almost the same interaction with both polymer components, causes more reduction in the scratch depth than sample R3.

In general, increasing the stiffness of the polymers enhances the scratch resistance; moreover, yield and tensile strength manage the plastic flow and other scratch damages like cracks and crazes.¹³ Although samples R6 and R7 have shown approximately the same elastic modulus ($E \sim 3000$ MPa) and tensile strength ($\sigma_y \sim 50$ MPa), more clay-contained sample, R7, introduces more recovery. Regardless of quality of the clay dispersion and location in these hybrid samples, it is revealed by DMA analysis at room temperature that storage modulus of sample R7 ($E_{R7}' = 1.6$ GPa) is greater than R6 ($E_{R6}' = 1.48$ GPa), whereas values of loss modulus are close to each other ($E_{R7}'' = 104.7$ MPa and $E_{R6}'' = 105$ MPa). Therefore, sample R7 will present more elastic behavior than sample R6, and as a result, higher scratch depth recovery.

CONCLUSIONS

The blends of ABS and PMMA and their hybrids with the addition of three different clays (Nanofil[®] SE3010 and Cloisite[®] 30B and 20A) were melt-processed in a corotating twin-screw extruder. The dispersion of clays in the polymeric blend was investigated using XRD and TEM. RSM was successfully used to analyze the tensile behavior. In the nanocomposites containing lower amount of C20A and C30B, the clays were observed to be mainly located at the interface of ABS/PMMA. Clay C30B appeared to show higher degree of intercalation, whereas clay SE3010 presented nonintercalated stiffened hybrids. All organoclays reduced the size of PMMA domains; however, clays C30B and C20A enhanced the ABS/PMMA adhesion and consequently improved the tensile strength. The incorporation of clays improved the compatibility of 90/10 ABS/PMMA blends and, consequently, increased the T_g s. However, the T_g of the nanocomposites containing higher amount of PMMA

were not affected by the clays. The blending of ABS with scratch-resistant PMMA improved the scratch resistance of ABS. Furthermore, the incorporation of 4 wt % of clay C30B caused more scratch depth recovery.

References

1. Scheirs, J.; Priddy, D. B. *Modern Styrenic Polymers: Polystyrene and Styrenic Copolymers*; Wiley: England, 2003.
2. Kim, Y. J.; Shin, G. S.; Lee, I. T.; Kim, B. K. *J Appl Polym Sci* 1993, 47, 295.
3. Kim, B. J.; Shin, G. S.; Kim, Y. J.; Park, T. S. *J Appl Polym Sci* 1993, 47, 1581.
4. Lee, S. M.; Choi, C. H.; Kim, B. K. *J Appl Polym Sci* 1994, 51, 1765.
5. Li, Q.; Tian, M.; Kim, D.; Zhang, L.; Jin, R. *J Appl Polym Sci* 2002, 85, 2652.
6. Han, C. D.; Yang, H. H. *J Appl Polym Sci* 1987, 33, 1221.
7. Fowler, M. E.; Barlow, J. W.; Paul, D. R. *Polymer* 1987, 28, 2145.
8. Suess, M.; Kressler, J.; Kammer, H. W. *Polymer* 1987, 28, 957.
9. Sinha, S. K.; Lim, D. B. *J Wear* 2006, 260, 751.
10. Adams, M. J.; Allan, A.; Briscoe, B. J.; Doyle, P. J.; Gorman, D. M.; Johnson, S. A. *Wear* 2001, 251, 1579.
11. Hicks, C. T.; Hoffman, R. D.; Thompson, J. E. U.S. Pat. 5069851, 1992.
12. Ha, D. H.; Jeong, B. J. U.S. Pat. 20090043047, 2009.
13. Dasari, A.; Yu, Z. Z.; Mai, Y. W. *Mater Sci Eng R* 2009, 63, 31.
14. Gwabaza, T.; Ray, S. S.; Focke, W. W.; Maity, A. *Eur Polym J* 2009, 45, 353.
15. Goitisolo, I.; Eguiazabal, J. I.; Nazabal, J. *Eur Polym J* 2008, 44, 1978.
16. Kim, H. B.; Choi, J. S.; Lee, C. H.; Lim, S. T.; Jhon, M. S.; Choi, H. *J Eur Polym J* 2005, 41, 679.
17. Lipatov, Y. S.; Nesterov, A. E.; Ignatova, T. D.; Nesterov, D. A. *Polymer* 2002, 43, 875.
18. Ginzburg, V. V. *Macromolecules* 2005, 38, 2362.
19. Khatua, B. B.; Lee, D. J.; Kim, H. Y.; Kim, J. K. *Macromolecules* 2004, 37, 2454.
20. Sung, Y. T.; Kim, Y. S.; Lee, Y. K.; Kim, W. N.; Lee, H. S.; Sung, J. Y.; Yoon, H. G. *Polym Eng Sci* 2007, 47, 1671.
21. Ray, S. S.; Pouliota, S.; Bousmina, M.; Utracki, L. A. *Polymer* 2004, 45, 8403.
22. Ray, S. S.; Bousmina, M.; Maazouz, A. *Polym Eng Sci* 2006, 46, 1121.
23. Mallick, S.; Dhibar, A. K.; Khatua, B. B. *J Appl Polym Sci* 2010, 116, 1010.
24. Martins, C. G.; Larocca, N. M.; Paul, D. R.; Pessan, L. A. *Polymer* 2009, 50, 1743.
25. Ozkoc, G.; Bayram, G.; Tiesnitsch, J. *Polym Compos* 2008, 29, 345.
26. Filippone, G.; Dintcheva, N. T.; La Mantia, F. P.; Acierno, D. *Polymer* 2010, 51, 3956.
27. Li, Y.; Shimizu, H. *Polymer* 2004, 45, 7381.
28. Si, M.; Araki, T.; Ade, H.; Kilcoyne, A. L. D.; Fisher, R.; Sokolov, J. C.; Rafailovich, M. H. *Macromolecules* 2006, 39, 4793.
29. Hong, J. S.; Kim, Y. K.; Ahn, K. H.; Lee, S. J.; Kim, C. *Rheol Acta* 2007, 46, 469.
30. Fang, Z.; Harrats, C.; Moussaif, N.; Groeninckx, G. *J Appl Polym Sci* 2007, 106, 3125.
31. Fenouillot, F.; Cassagnau, P.; Majeste, J. C. *Polymer* 2009, 50, 1333.
32. Hong, J. S.; Kim, Y. K.; Ahn, K. H.; Lee, S. J. *J Appl Polym Sci* 2008, 108, 565.
33. Mederic, P.; Ville, J.; Huitric, J.; Moan, M.; Aubry, T. *Polym Eng Sci* 2011, 51, 969.
34. Vo, L. T.; Giannelis, E. P. *Macromolecules* 2007, 40, 8271.
35. Lee, M. H.; Dan, C. H.; Kim, J. H.; Cha, J.; Kim, S.; Hwang, Y.; Lee, C. H. *Polymer* 2006, 47, 4359.
36. Shumsky, V. F.; Getmanchuk, I.; Ignatova, T.; Maslak, Y.; Cassagnau, P.; Boiteux, G.; Melis, F. *Rheol Acta* 2010, 49, 827.
37. Xiao, J.; Hu, Y.; Lu, H.; Cai, Y.; Chen, Z.; Fan, W. *J Appl Polym Sci* 2007, 104, 2130.
38. Wang, S.; Hu, Y.; Wang, Z.; Yong, T.; Chen, Z.; Fan, W. *Polym Degrad Stab* 2003, 80, 157.
39. Wang, K. H.; Choi, M. H.; Koo, C. M.; Choi, Y. S.; Chung, I. J. *Polymer* 2001, 42, 9819.
40. Hemati, F.; Garmabi, H. *Can J Chem Eng* 2010, 89, 187.
41. Rybnicek, J.; Lach, R.; Lapcikova, M.; Steidl, J.; Krulis, Z.; Grellmann, W.; Slouf, M. *J Appl Polym Sci* 2008, 109, 3210.
42. Vaia, R. A.; Giannelis, E. P. *Macromolecules* 1997, 30, 8000.
43. Pavlidou, S.; Papaspyrides, C. D. *Prog Polym Sci* 2008, 33, 1119.
44. Patinosoto, A. P.; Valdes, S. S.; Ramosdevalle, L. F. *J Polym Sci Part B: Polym Phys* 2008, 46, 190.
45. Tiwari, R. R.; Natarajan, U. *J Appl Polym Sci* 2008, 110, 2374.
46. Kumar, S.; Jog, J. P.; Natarajan, U. *J Appl Polym Sci* 2003, 89, 1186.
47. Stretz, H. A.; Paul, D. R.; Cassidy, P. E. *Polymer* 2005, 46, 3818.
48. Lee, M. H.; Lee, K. H.; Min, B. H.; Kim, J. H. *J Appl Polym Sci* 2010, 117, 49.
49. Filippone, G.; Dintcheva, N. T.; La Mantia, F. P.; Acierno, D. *J Polym Sci Part B: Polym Phys* 2010, 48, 600.
50. Chen, G. X.; Kim, H. S.; Kim, E. S.; Yoon, J. S. *Polymer* 2005, 46, 11829.
51. Kusmono, S. T.; Mohd Ishak, Z. A.; Chow, W. S.; Takeichi, T.; Rochmadi, D. *Compos A* 2008, 39, 1802.
52. Nayak, P. L.; Sasmal, A.; Nayak, P.; Sahoo, S.; Mishra, J. K.; Kang, S. C.; Lee, J. W.; Chang, Y. W. *Polym Plast Technol Eng* 2008, 47, 600.
53. Kumaraswamy, G. N.; Ranganathaiah, C.; Deepa Urs, M. V.; Ravikumar, H. B. *Eur Polym J* 2006, 42, 2655.
54. Dasari, A.; Yu, Z. Z.; Mai, Y. W. *Acta Mater* 2007, 55, 635.